CHALMERS
UNIVERSITY OF TECHNOLOGY

Implementation of a sub-and supercritical carbon dioxide process for the selective recycling of the electrolyte from spent Li-ion battery

Journal of CO2 Utilization 81 (2024) 102703

Contents lists available at ScienceDirect

Journal of CO2 Utilization

journal homepage: www.elsevier.com/locate/jcou

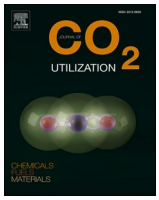

Implementation of a sub-and supercritical carbon dioxide process for the selective recycling of the electrolyte from spent Li-ion battery

Nils Zachmann [a,*], Robert V. Fox [b], Martina Petranikova [a], Burçak Ebin [a]

[a] Department of Chemistry and Chemical Engineering, Chalmers University of Technology, Kemivägen 4, SE-412 96 Gothenburg, Sweden
[b] Materials Separations and Analysis, Idaho National Laboratory, Idaho Falls, ID 83415, United States

ARTICLE INFO

Keywords:
Lithium-ion battery
Electrolyte
Recycling process
Supercritical carbon dioxide extraction
Spectroscopy analysis
Exhaust-gas emission characterization

ABSTRACT

The electrolyte in spent Li-ion batteries is prone to cause a high risk of hazardous emissions (HF, etc.) in the state-of-the-art recycling processes. It is the main source of fire risks and represents a significant burden for the recyclers due to the safety. Still, extended research to fully recycle the electrolyte without its destruction at elevated temperature is scarce. This study focuses on the electrolyte extraction from spent LiBs using sub- and supercritical carbon dioxide to fill this gap. The effects of the critical process parameters, pressure (60–120 bar), temperature (15–55 °C) and extraction time (1–50 min) from spent pouch cells were investigated. The results showed that the CO_2 density, which is related to pressure and temperature, is significant for the recovery of the non-polar electrolyte solvents. The most important outcome is that dimethyl carbonate, and ethyl methyl carbonate were fully selectively extracted at the studied conditions, whereas the polar ethylene carbonate was extracted only in trace amounts. As results indicated, $LiPF_6$ did not decompose in the proposed process whereby the toxic-gas emissions were dramatically minimized compared to the state-of-the-art recycling processes.

1. Introduction

In lithium-ion batteries (LiBs) the electrolyte is one of the most crucial component for the cell performance during its service life and corresponds to 10–20 wt percent of the LiB cell [1–3]. The state-of-the-art non-aqueous liquid electrolyte is a multi-component system composed of a conductive Li-salt, organic solvents, and potential additives [4]. Lithium hexafluorophosphate ($LiPF_6$), which is the most commonly used conductive salt, is dissolved in a mixture of linear and cyclic carbonates such as dimethyl carbonate (DMC), ethyl methyl carbonate (EMC), diethyl carbonate (DEC), propylene carbonate (PC), and/or ethylene carbonate (EC) [1,4–6]. The electrolyte solvents are the largest proportion of the electrolyte mixture whether by weight or volume. The most common additives are vinyl carbonate (VC), fluoroethylene carbonate (FEC), or tris(trimethylsilyl)phosphite (TMSPi) but a wide range of additives can be added to adjust the electrolyte properties [5].

A lot of attention in research and industry is devoted towards the design of the electrolyte to improve the performance, safety, lifetime, and cost of the LiB cell. Up to today, recycling of electrolyte is seldomly considered in industrialized recycling strategies as the focus is rather on the recovery of the valuable metals present in the cathode active materials (Li, Co, Mn, Ni) [7–9]. Conventional recycling processes include a pre-treatment step, consisting of thermal treatment for the removal of the electrolyte, the polymer binder material, the separator, and other organics to eventually liberate the active material and produce a black mass for the hydrometallurgical recovery of the valuable metals [7]. Thereby, the volatile and inflammable electrolyte solvents evaporate and the thermally unstable $LiPF_6$ decomposes forming fluorinated toxic gas emissions (HF, POF_3, etc) [10–15]. Despite its low economical value compared to the valuable cathode metals, the safe removal of the electrolyte is essential from an environmental point of view, since it reduces the greenhouse gas emissions generated by the incineration of the electrolyte as well as the threats associated with the LiB waste, while increasing the safety of the overall recycling process [16]. The indirect economic benefit of the electrolyte recovery should also be considered. Any incurred costs related to the complex removal of the organics in accumulated waste streams, i.e., in the process water of the hydrometallurgical process, can be potentially reduced [17,18].

A few research groups focussed on the recycling of the electrolyte using methods such as vaporization processes, organic solvent extraction and supercritical fluid technology [7,19–22]. Among those, the

* Corresponding author.
E-mail address: zachmann@chalmers.se (N. Zachmann).

https://doi.org/10.1016/j.jcou.2024.102703
Received 11 October 2023; Received in revised form 9 February 2024; Accepted 10 February 2024
Available online 14 February 2024

supercritical fluid technology is predestinated for the electrolyte recycling because of the excellent mass transfer characteristics i.e. the quick spread of the solvent, neglectable surface tension, penetration into the solute matrix, faster dissolution times, and easy removal from the solute matrix by simply reducing the pressure [23]. CO_2 is often chosen as a solvent due to its low critical pressure and temperature (73.8 bar, 31 °C) as well because it is non-flammable, cheap, reusable, non-toxic, and, abundant [23–26]. Supercritical CO_2 ($scCO_2$) is generally classified as a non-dipolar solvent being a good solvent for many non-polar compounds [27]. Thus, under variation of the extraction conditions pressure and temperature, the extraction of the non-polar linear carbonates can be highly selective. However, the extraction of the cyclic carbonates and conductive salt can be challenging under readily achievable pressure and temperature conditions as $scCO_2$ is known to be a poor solvent for high molecular weight polymers and ionic compounds of high polarity. It is well-established in the literature that CO_2 can act as both a weak Lewis acid and base and can participate in conventional and nonconventional hydrogen-bonding interactions [28,29]. In our study we use these properties to selectively extract the electrolyte compounds from the LiB sample.

According to literature, the extraction of the different electrolyte solvents and $LiPF_6$ is sensitive to the process conditions pressure, temperature, the extraction mode (static and dynamic extraction) and the extraction material [30–33]. A combination of static and dynamic extraction mode has been reported to be beneficial to achieve high electrolyte extraction yields [31,33]. Variations in temperature (30–50 °C) and pressure (150–350 bar) were reported to cause a similar trend for the extraction of non-polar electrolyte solvents (DMC, and EMC) from a polypropylene separator which was soaked with synthetic TC-E201# electrolyte (EC, DMC, EMC, $LiPF_6$) [32]. Grützke et al. [31] reported that the electrolyte extraction yield from cylindrical (18650) LiB jelly rolls was almost doubled when an additional co-solvent was used compared to pure liquid CO_2 (60 bar, 25 °C) and $scCO_2$ (300 bar, 40 °C). Thereby, DMC, and EMC were quantitatively recovered and the polar components EC, and $LiPF_6$ were qualitatively recovered. There is still a lack of investigation of the electrolyte separation yield from spent EV batteries (pouch cells) under variation of temperature and pressure conditions using mild pressures below 150 bar.

In this study, the effects of different critical process parameters to extract the electrolyte solvents from spent LiB pouch sub – and $scCO_2$ technology were investigated. Special attention was paid to the effects of static and dynamic extraction times (0–50 min), pressure (60–120 bar), temperature (15 - 55 °C) and corresponding CO_2 process densities. The composition of the collected extract was qualitatively and quantitively determined. Moreover, the process exhaust gas stream was continuously analyzed towards its toxic composition and the impact of the process on the active cathode material for subsequent recycling steps for the recovery of the valuable transition metals was studied.

2. Experimental section

2.1. Materials and reagents

Discharged spent NMC/graphite LiB pouch cells produced for an EV application were used in this study. In a previous study, the pouch cell electrolyte was determined to be based on EC/DMC/ EMC solvents (approx. 1:1:1 v/v), and $LiPF_6$ [34]. Liquid carbon dioxide (CO_2) with a purity of ≥ 99.99% (H_2O ≤5 ppm w/w) was purchased from Air Liquide. HNO_3 (>65%), acetone (>95%), acetonitrile (>99.9%), ethylene carbonate (>99.9%), and dimethyl carbonate (>99%) were purchased from Merck Millipore and dry ice from Cryotech.

2.2. Experimental procedures

2.2.1. Sample preparation

The discharged spent NMC battery pouch cells were stored for 2 days at - 18°C to minimize the evaporation of the volatile electrolyte solvent during the cell opening procedure. The pouch of the battery cell was opened by slicing along its edges with a sharp knife to remove the electrode stack (several layers of anode, separator, and cathode). A scalpel was used to cut rectangular pieces of the electrode stack with dimensions of 14.7 × 0.5 cm (8.81 ± 0.72 g). Between each subsequent experimental run, the remaining electrode stack was placed inside a sealed bag and returned to the storage at - 18 °C.

2.2.2. Set-up

The supercritical fluid technology system used in this work, as illustrated in Fig. S1, was constructed inside a fume hood. A syringe pump system (ISCO 260D, Teledyne ISCO) was used to pressurize liquid CO_2 (99.9%) to the process conditions and the syringe pump temperature was thermostated using an external heat system (Model F10 & CM, Julabo). The CO_2 flow into the stainless-steel extractor (7.5 ml) was directed by manual valves and the pressure monitored with a manometer. The temperature was controlled using an extensively whirled water pipe along the extractor which was connected to an external thermostat (Model F12 & ED, Julabo) and monitored using a thermocouple connected to a data logger (TC-08, Pico Technology). The flow rate was controlled by a metering valve. To avoid freezing the outlet, the exhaust metering valve temperature was stabilized to 40 ± 5 °C by a thermostat. The process exhaust was passed through a sample vial placed in a cold trap containing a mixture of dry ice and acetone (−78 °C) to collect the extracted electrolyte. A gas collection chamber situated inside a Fourier-transform infrared spectrometer was connected to the cold trap outlet for the analysis of the exhaust emission. After bubbling through a gas washing bottle, which was filled with 50 ml MQ water, the exhaust gas was released to the environment. In the future, the clean CO_2 exhaust can be reused in the sub- and $scCO_2$ extraction process.

2.2.3. Method

The sample was inserted into the extractor and the extractor leak-tight closed using wrenches. The water pipes were then extensively whirled along the extractor to stabilize the process temperature (15-55 °C with uncertainties of 2°C). The extractor was pressurized to the process pressure (60 - 120 bar with uncertainties of 4 bar) using the syringe pump. Two different extraction modes, static and dynamic extraction, were applied and investigated. In the static extraction mode, the pressure and temperature conditions were kept constant without a CO_2 flow and the CO_2 was released after the extraction time. In the dynamic extraction mode, a constant CO_2 flow was applied throughout the entire extraction time while keeping pressure and temperature conditions constant. After pre-liminary experiments the following CO_2 extraction process was applied. A static equilibration time of 3 min was used to stabilize the system. Then a constant CO_2 flow (1.0 ± 0.2 L/min, outlet flow at 25 °C and room pressure) was applied for 30 min. After the extraction time, the extractor was entirely depressurized, the water pipes removed, the extractor opened, and the sample removed. The weight of the LiB sample was determined before and after the experimental run using a precision scale (resolution 0.01 mg and linearity ± 0.1 mg). All experiments were conducted in triplicates. The cold trap outlet exhaust was frequently monitored in the range of 4000–900 cm^{-1} over the entire process time using Fourier-transform infrared spectroscopy (FTIR).

The collected extract was analyzed by attenuated total reflection (ATR)-FTIR, gas chromatography coupled with mass spectroscopy (GC-MS), and inductively coupled plasma optical emission spectroscopy (ICP-OES) to determine its composition and elemental impurities. For the ATR-FTIR analysis 200 µl of the collected extract was placed on top of the diamond surface of the universal ATR accessory. GC-MS analysis was performed after the sample was diluted in acetonitrile (150:1 dilutant to stock). For ICP-OES analysis the collected extract was diluted in 0.5 M HNO_3 (80:1dilutant to stock) and subsequently filtered.

The active cathode material was scraped from the current collector

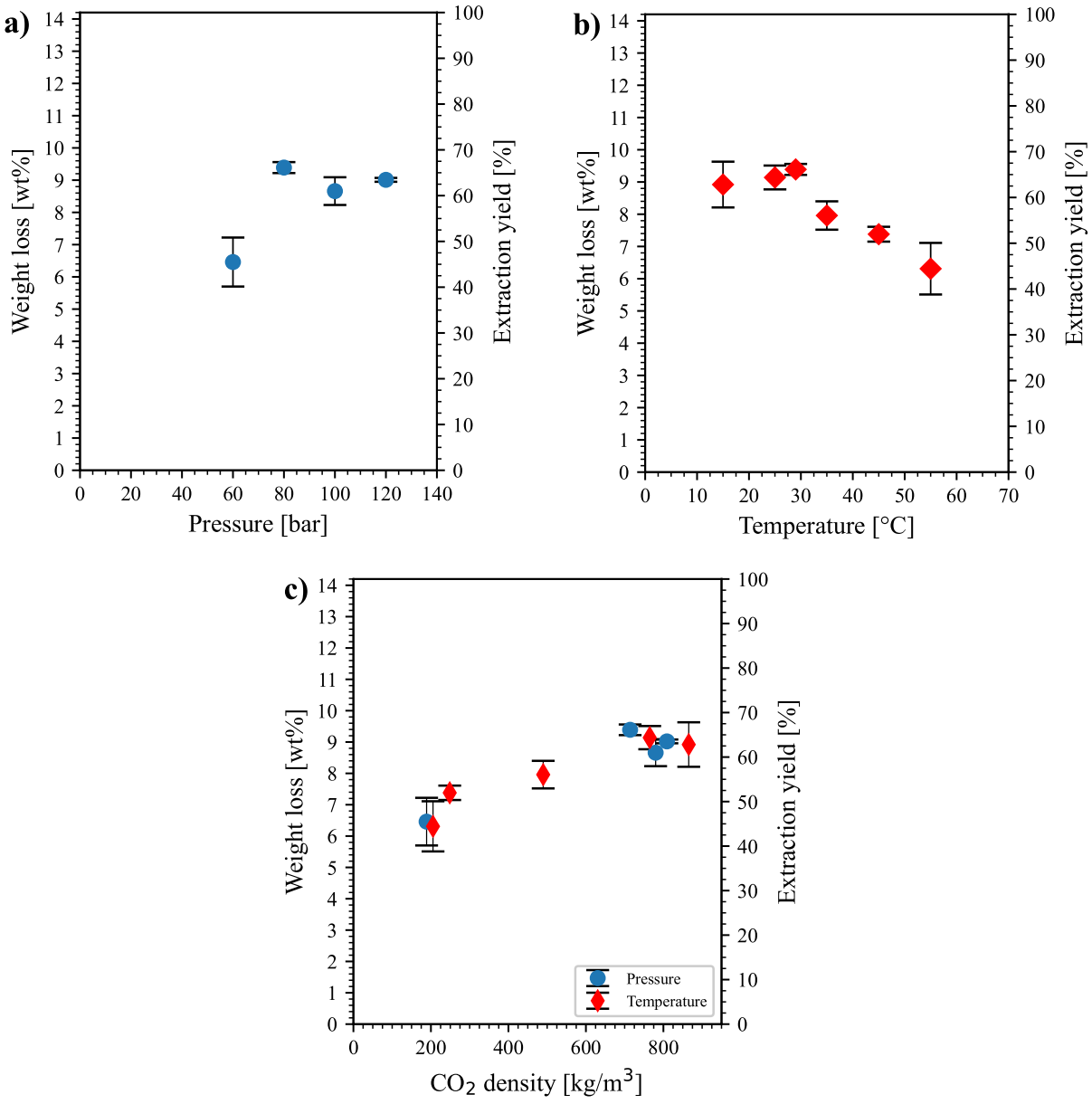

Fig. 1. : LiB sample weight loss in weight percentage [wt%] after the sub- and $scCO_2$ extraction process at different process parameters, a) dependence of pressure at 29 °C, b) dependence of temperature at 80 bar c) dependence of CO_2 density. The error bars in the plots represent the standard deviations (1σ) of the triplicates at each process condition.

using a razor blade for X-ray diffraction (XRD) analysis and was collected in a sample vial. After adding acetone, the cathode active material powder was brought into suspension using sonication. The sample was then coated on the surface of a silicon crystal sample holder by dropping a few droplets in its centre. The sample was dried by evaporating the acetone and the process was repeated until an evenly coated surface was achieved on the crystal sample holder.

2.3. Measurement and characterization

The electrode stack sample weight loss was associated with the amount of the extracted electrolyte in the process. The sample weight loss in weight percent (wt%) after the CO_2 extraction process was calculated according to Eq. (1):

$$Weight\ loss = \left(1 - \frac{m_{after}}{m_{initial}}\right) \times 100 \quad (1)$$

where $m_{initial}$ is the initial sample weight and m_{after} is the sample weight after the CO_2 extraction process. Based on the sample weight loss, the extraction yield was then estimated. The total weight percent of the electrolyte in the electrode stack sample was estimated to be 14.2 wt% based on previous published results [34]. The share of $LiPF_6$ in the total electrolyte amount was estimated to be 11.8%, which corresponds to 1.7 wt% of electrode stack.

GC-MS (7890 A, Agilent Technologies) with an Agilent HP-5MS 5% Phenyl Methyl Silox column (30 m x 250 μm x 0.25 μm) was used to analyze the collected extract. The samples were automatically injected with a split ratio of 1:100 and a 3 ml/min purge flow at 250 °C. Helium was selected as carrier gas and the column flow was set to 1 ml/min. The initial column oven temperature (40°C) was held for 1 min and then increased with a heat rate of 20°C/min to the final oven temperature (230 °C). Finally, the final oven temperature was held for 2 min. The electron ionization mode (EI) with an ion source temperature of 230°C

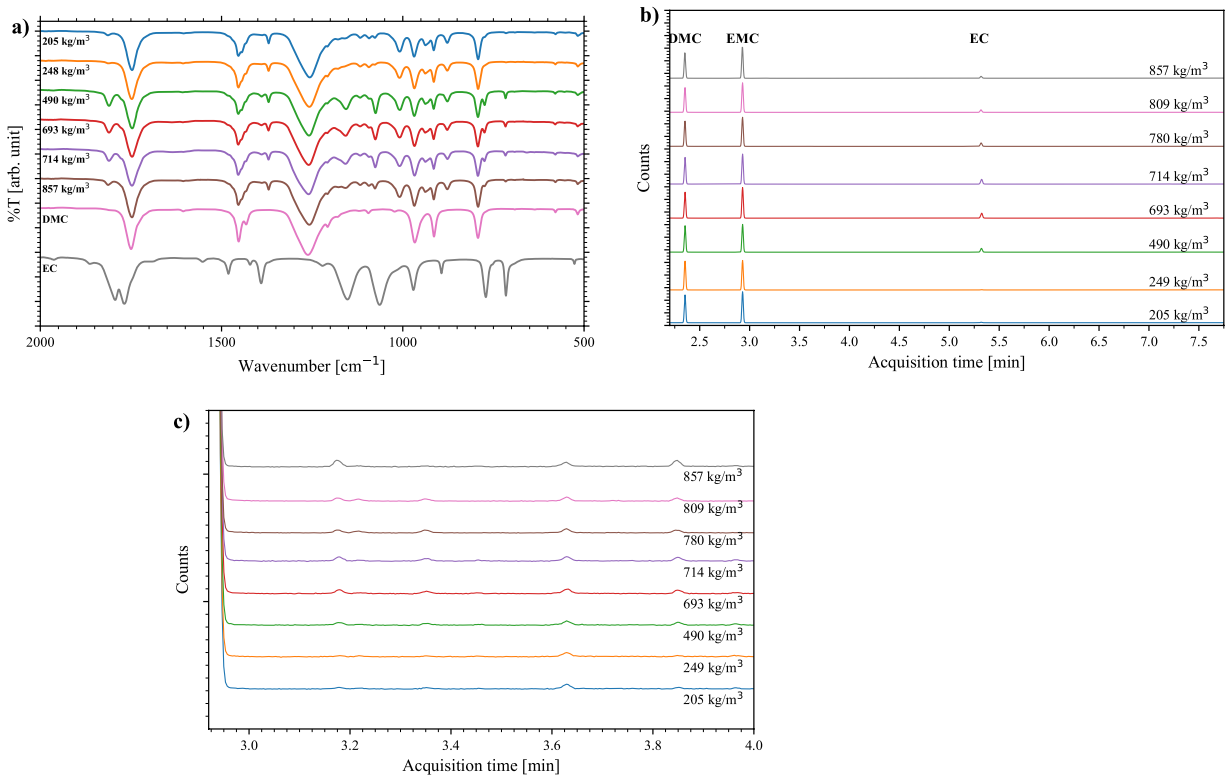

Fig. 2. : (a) ATR-FTIR spectra of the collected extract at various CO_2 densities together with pure liquid phase DMC, and EC as a reference. (b) GC-MS chromatogram of the recovered liquid phase product at various CO_2 densities and (c) focused between 2.9 and 4 min.

and 70 eV filament voltage was chosen to obtain the mass spectrum in a range of 15–300 *m/z*.

ICP-OES (ThermoFisher Scientific, iCAP PRO) was used for elemental analysis of the collected extract. Standards containing Li, Ni, Co, Mn, Fe, Cu, Al, P, and Zn were prepared by dilution in 0.5 M HNO_3 for the linear range calibration between 0.625 to 20 ppm. In the used method, the approximate limit of detection was 0.1 ppm.

The universal attenuated total reflection method of the FTIR spectrometer (Spectrum Two, Perkin Elmer) was used to characterize the collected extract and the reference spectra of DMC, and EC in liquid phase. The ATR-FTIR spectra were recorded in a range between 4000 cm^{-1} and 450 cm^{-1} with a resolution of 2 cm^{-1} and a total of 4 scans.

The process exhaust gas was passed through a gas collection chamber and continuously analyzed by FTIR (Spectrum Two, Perkin Elmer). The In-Situ FTIR spectra were recorded with a scan rate of 16 scans in the range of 4000 cm^{-1} to 900 cm^{-1} and a resolution of 4 cm^{-1}.

X-ray diffraction analysis (XRD, Bruker D8 Discover, EIGER2R 500 K detector) was used to analyze potential structural changes of the active cathode material before and after the electrolyte extraction process in a 2Θ range of 10° - 80° the range. A Cu radiation source with a characteristic K_α wavelength of 1.5406 Å was used and the operating voltage and current were set to 40 kV and 40 mA.

3. Results and discussions

The influence of the extraction time in static, dynamic and a combination of static and dynamic extraction was studied in preliminary experiments using process conditions at 80 bar and 29 °C and the results are presented in Fig. S2. The weight loss of the electrode stack sample was associated with the amount of extracted electrolyte. Prolonging the static extraction time had no significant effect on the electrolyte extraction yield as seen as in Fig. S2a. The dynamic extraction time, on the contrary, was significant for the extraction of the electrolyte from the electrode stack sample. As seen in Fig. S2b, the electrolyte extraction yield increased along with the dynamic extraction time before reaching a plateau after 30 min. Additionally, the influence of the static extraction time with a fixed dynamic extraction time of 30 min was studied and the results plotted in Fig. S2c. As observed before, an increase of the static extraction time had no impact for the electrolyte extraction yield. According to literature, the dynamic extraction mode is favored when the solute is weakly bound to the sample matrix and the solvent-solute equilibrium can be reached rather fast [23,35,36]. This is the case especially for the volatile electrolyte components DMC, and EMC. The results were also in accordance with the studies by Grützke et al. and Mu et al. which reported higher extraction yields using dynamic extraction compared to static extraction [31,33].

The effect of pressure (60–120 bar) at constant temperature (29°C) and constant CO_2 flow is plotted in Fig. 1a. It can be observed that the maximum electrolyte extraction yield of 66% (9.4 ± 0.2 wt%) was achieved at 80 bar. The electrolyte extraction yield decreased slightly to 64% (9.0 ± 0.7 wt%) at higher pressures (i.e., 120 bar). Fig. 1b shows that an increase in process temperature above 29 °C resulted in a (linear) electrolyte extraction yield decrease. At 29 °C and below, the electrolyte extraction yield remained constant with respect to the standard deviation of the triplicate. Mu et al. [33] reported a similar temperature effect at 70 bar while using an electrolyte-soaked separator as extraction medium and a different electrolyte solvent composition (EC, PC, DMC, EMC). Liu et al. [32] reported a small electrolyte extraction yield increase from an electrolyte-soaked separator while the process temperature was increased (30–50°C) at 250 bar.

The observed effect of pressure and temperature on the extraction yield reflects the importance of the CO_2 density for the electrolyte extraction. Typically, the solvation characteristics in $scCO_2$ are highly related to its density as the specific solvent-solute interaction probability increases with an increase in CO_2 density [37]. At a given temperature an increase in pressure results in an increased CO_2 density leading to an increase of the solvation power. The temperature effect for the solvation

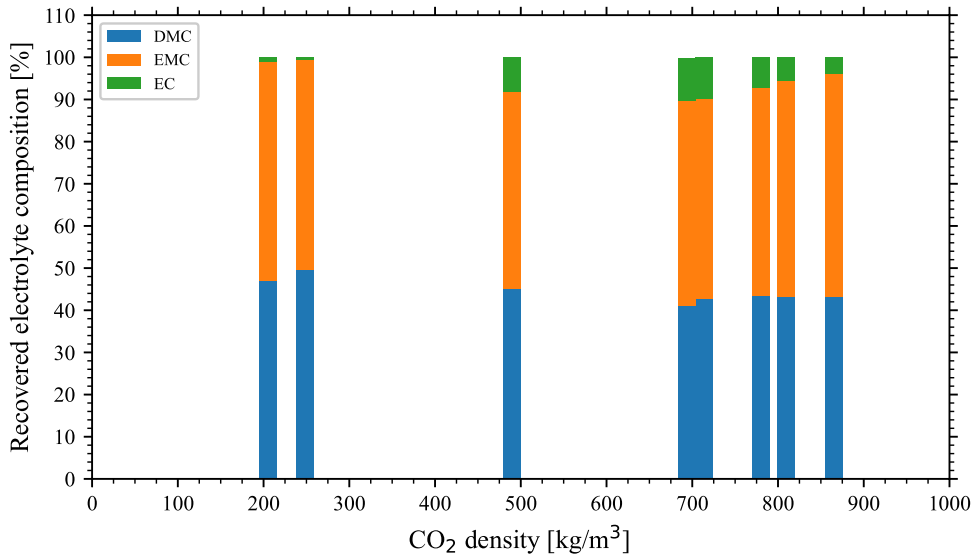

Fig. 3. Composition of the collected extract obtained at various CO_2 process densities based on the GC-MS analysis.

processes in $scCO_2$ is more complex, especially for low volatile solutes since the effect of the solute vapor pressure and kinetics compete with the effect of the CO_2 density. At a given pressure, an increase of temperature leads to a decrease of the solvent density and thus the probability of solute-solvent interactions decreases. Meanwhile, the solute vapor pressure and the kinetics of solvent-solute interaction increase which leads to a competing effect what is termed the cross-over effect. Below the cross-over pressure, the solvent density effect is dominant, and the solvation power decreases with an increase in temperature at a given pressure. Above the cross-over pressure, the CO_2 density changes are no longer remarkably significant, and the solute vapor pressure and kinetic effects become dominant, and the solvation power increases with temperature [23,37]. At the studied pressure condition, a decrease in electrolyte separation yield was observed while the process temperature was increased. This implies that at the studied pressure conditions the controlling factor in electrolyte extraction was the CO_2 density.

To verify the importance of the CO_2 density for the electrolyte extraction at the studied extraction conditions, the CO_2 density for the applied process conditions were estimated [38] and plotted against the corresponding estimated electrolyte extraction yield in Fig. 1c. As expected, a clear dependence of the electrolyte extraction yield on the CO_2 density was observed. The extraction yield increased remarkably with an increase in CO_2 density until a CO_2 density of 700 kg/m^3 was reached. At CO_2 densities above 700 kg/m^3 the electrolyte extraction yield was rather constant with respect to the standard deviation of the triplicates with the highest achieved electrolyte extraction yield of 66% at a CO_2 density of 715 kg/m^3.

The composition of the collected extract was analyzed with ATR-FTIR, GC-MS, and ICP-OES. Fig. 2a shows the ATR-FTIR spectra of the collected extract at various extraction conditions in the range between 2000–500 cm^{-1} along with the spectra of the electrolyte solvents DMC, and EC serving as a reference. Vibrational peaks associated with DMC, and EC were clearly observed in the collected extract while remarkable compositional changes within the different electrolyte extraction conditions were not observed. However, due to intermolecular interactions between the organic carbonates in liquid phase, changes in peak positions can occur and the qualitative analysis cannot be taken for granted. However, in combination with GC-MS analysis, the composition of the electrolyte can be analyzed qualitatively and quantitively.

Selected GC-MS chromatograms of the collected extract at various

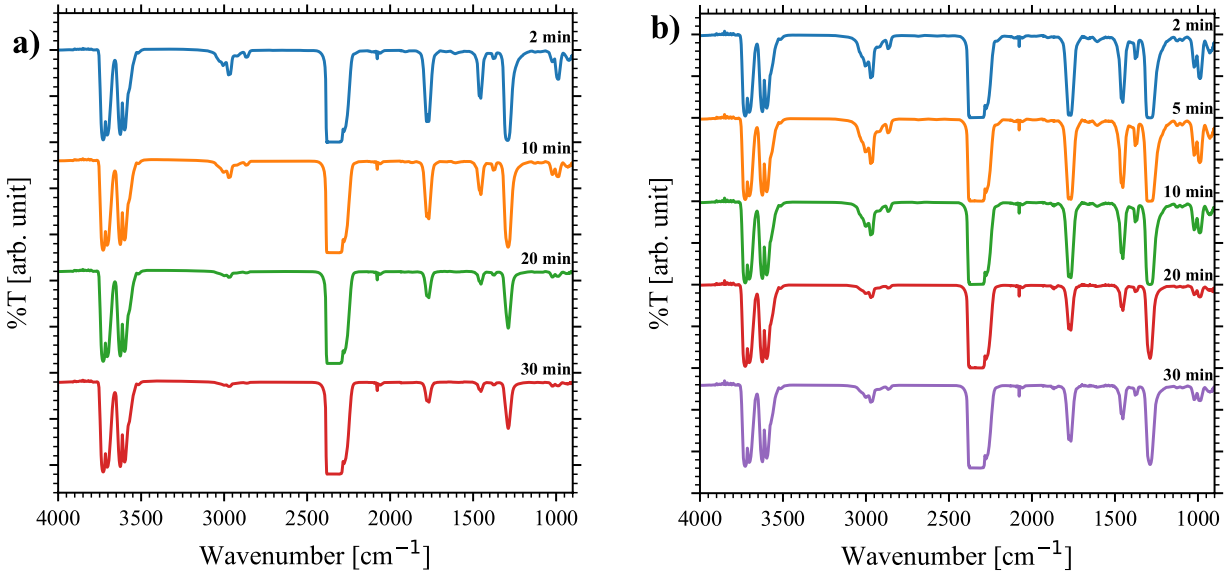

Fig. 4. : FTIR spectra of the process exhaust gas-emission at various process times a) after and b) before the cold trap at a CO_2 density of 715 kg/m^3.

CO_2 densities are plotted in Figs. 2b and 2c. The GC-MS analysis confirmed that the collected extracts were mainly composed of DMC (2.35 min), EMC (2.93 min), and EC (5.31 min). In addition, minor peaks at 3.18, 3.35, 3.63, and 3.85 min were observed. The peaks at 3.18 and 3.85 min were assigned to the electrolyte decomposition products dimethyl fluorophosphate (DMFP), and ethyl methyl fluorophosphate (EMFP) [39]. The peaks at 3.35 and 3.63 min were assigned to VC and DEC. VC is a well-known electrolyte additive and DEC was formed via a transesterification reaction from EMC [4,40].

The results of the quantitative analysis of the GC-MS results are plotted in Fig. 3. Regardless of the process condition, the collected extracts were mainly composed of the linear carbonates DMC, and EMC with a share of more than 90%, whereas only minor amounts of the cyclic EC (<10%) were present. At densities below 300 kg/m^3 the share of EC in the collected extract was less than 2% and slightly increased up to 10% at a CO_2 density of 715kg/m^3. Elemental impurities of the collected extract were analyzed using ICP-OES. The Li concentration was below the detection limit of the instrument, but P (362 ± 65 mg/L), and Al (5.2 ± 0.4 mg/L) were detected at all process conditions. The other measured elemental concentrations (Ni, Co, Mn, Fe, Cu, and Zn) were all below the detection limit. Assuming a state-of-the-art 1 M $LiPF_6$ concentration in the electrolyte solution, the P amount corresponded to only trace amounts (<1.2%) of $LiPF_6$. Considering that Li was below the detection limit, it is believed that P in the collected extract originated from the electrolyte aging products, such as the detected DMFP, and EMFP in the GC-MS analysis [40,41].

It is important to highlight that the collection yield of the extracted electrolyte was around 60%. Thus, the composition of the collected extract given in Fig. 3 is not representative of the share of the actual extracted electrolyte. To investigate the composition of the uncollected extracts, the cold trap exhaust was frequently analyzed during the entire process time with FTIR, and the results for the CO_2 extraction condition with a density of 715 kg/m^3 are plotted in Fig. 4a. This condition was selected as it yields the highest electrolyte extraction amount. Strong CO_2 vibration peaks (3728 cm^{-1}, 3704 cm^{-1}, 3624 cm^{-1}, 3599 cm^{-1}, 2349 cm^{-1} (broad)) and weak peaks belonging to carbon monoxide (around 2075 cm^{-1}) were observed at all process times, which originated from the extraction medium CO_2. As a reference, the FTIR spectrum of pure CO_2 is plotted in Fig. S3. In addition, vibrational peaks associated with DMC (1780 cm^{-1} (νC═O), 1463 cm^{-1} (CH_3 sym. def.), and 1295 cm^{-1} (ν_aO-C-O)) and EMC (1772 cm^{-1} (νC═O), 1378 cm^{-1} (CH_3) and 1370 cm^{-1}) were detected in the cold trap exhaust stream whereas vibrational peaks belonging to EC (1876 cm^{-1}, 1868 cm^{-1}, and 1860 cm^{-1}) were not observed [34]. The FTIR spectra of the exhaust gas emissions before the extract collection in the cold trap is plotted in Fig. 4b. In addition to the vibrational peaks of DMC, and EMC, characteristic peaks of EC were detected this time. Thus, EC was believed to be fully collected in the cold trap due to the absence of the vibrational intensities. However, the cold trap exhaust gas analysis revealed the inefficient collection of the linear carbonates DMC, and EMC. Therefore, it can be concluded that the actual share of EC of the total extracted electrolyte is much lower at the studied conditions than indicated in Fig. 3.

In both FTIR spectra in Fig. 4, vibrational peaks corresponding to the $LiPF_6$ decomposition products HF (4000 cm^{-1} to 3600 cm^{-1}) and POF_3 (1428 cm^{-1}, 1416 cm^{-1}, 1404 cm^{-1} and 991 cm^{-1}) were not observed. This is an indication that $LiPF_6$ did not decompose in the studied process conditions. However, it should not be neglected that trace amounts of P (362 ± 65 mg/L) were detected in all collected extracts and the fluoro-organophosphates DMFP, and EMFP were observed in the GC-MS analysis. In the presence of organic carbonate solvents, $LiPF_6$ is very sensitive to decomposition into HF, POF_3, and LiF even at low humidity conditions or traces of water [42]. POF_3 then hydrolyzes or reacts with electrolyte solvents to form a variety of inorganic phosphates or organophosphates [41]. These reactions are also prone to occur during the ageing of the LiB cell. The liquid CO_2 used in this study had a purity of 99.99% with less than 5 ppm (w/w) H_2O. Moreover, moisture/humidity was absorbed during the sample preparation process, and the water vapor froze on the sample surface during the storage of the cell at − 18 °C. Thus, it should not be ruled out that electrolyte decomposition occurred during the proposed electrolyte recovery process.

The electrolyte in the pouch cell was estimated to be based on DMC/EMC/EC (1:1:1, v/v) electrolyte solvent. As seen in Fig. 3, acyclic ester carbonates (DMC, EMC) were much better extracted than the cyclic ester carbonate EC as well as the conductive salt, $LiPF_6$, at the studied conditions. CO_2 is a non-dipolar solvent with two active bond dipoles which can participate in weak Lewis acid-base interactions [29]. Carbonyl groups with their lone electron pair oxygen were reported to be CO_2-phillic and enhance the solubility of solutes in scCO_2 [28,43]. High solvation of esters in scCO_2 have been ascribed to LA-LB interactions between the carbonyl oxygen atom acting as the Lewis-base and the C atom of the CO_2 molecule acting as the Lewis-acid. An additional solvation site for CO_2 molecules may be provided by the ester oxygen leading to a greater attractive energy compared to a simple ketone and was shown to play a key role to form complexes between esters and CO_2 molecules [44,45]. Cooperative hydrogen interaction between the O atom of the CO_2 molecule and the methyl group of the solvating compound were believed to further reinforce the weak LA-LB interactions [29]. The lower extraction yield of the EC may be attributed to its higher polarity compared to the linear carbonates DMC, and EMC and the limitation for CO_2 molecules to cluster around the EC molecule to eventually form coordination rings. A higher solubility of CO_2 in linear carbonates (DMC, EMC, DEC) compared to cyclic carbonates (EC, PC) at atmospheric pressure was reported in literature [46]. Moreover, with its comparable large dielectric constant ($\varepsilon = 89.78$), EC was reported in literature to dominate the first Li^+ solvation sphere as it coordinates extensively with the Li^+ cation. In turn, DMC ($\varepsilon = 3.11$) and EMC ($\varepsilon = 2.96$) with their relatively low dielectric constants are rather pushed into the outer solvation sphere where they mainly decrease the viscosity of the electrolyte mixture [47]. The occupation of the CO_2-phillic carbonyl group of the EC molecule due to its coordination with the Li^+ cation may potentially further limit the of the CO_2 extraction ability of EC. Binary liquid-vapor equilibrium (LVE) phase diagrams for DMC-CO_2 [48–53], EMC-CO_2 [48], and DEC-CO_2 [54] have been reported in literature, which can be also used to explain the extraction behavior at the different operation conditions in this study. However, it must be emphasized that the binary VLE phase diagrams only function as an indication as the electrolyte is a multicomponent mixture, and the phase behavior is likely to be influenced by the other components present in the mixture. In the binary DMC-CO_2 phase diagrams, the critical mixture pressure increases with temperature and a phase envelope shift towards the left can be observed. At operating pressures of 80 bar and higher, DMC, and CO_2 can be assumed to be present in a single phase at all temperatures below 40 °C. At the selected operating temperatures of 45 °C, and 55 °C and a pressure of 80 bar, DMC, and CO_2 are likely to be present in the two-phase zone. An analog VLE phase behavior was published for the binary mixture of EMC-CO_2, and DEC-CO_2. The shift from single-phase to a two-phase region at temperatures above 40 °C and 80 bar serves as an explanation for the observed decrease in extraction yield as the solubility decreased.

After the extraction process, the sample was manually separated into the cathode, anode, and separator materials. A white residue was clearly observed on the surface of the cathode and separator material as seen in Fig. S4. ATR-FTIR analysis showed that the white residue was mainly composed of EC. This indicates that the non-extractable EC precipitated and remained in the sample after the extraction at the studied conditions.

According to our results, selective extraction of the acyclic DMC, and EMC without the generation of toxic gas emissions (HF, POF_3) at CO_2 densities between 600–900 kg/m^3 is possible. The remaining polar electrolyte components EC, and $LiPF_6$ can be potentially extracted in subsequent extraction steps using a supporting co-solvent. Grützke et al.

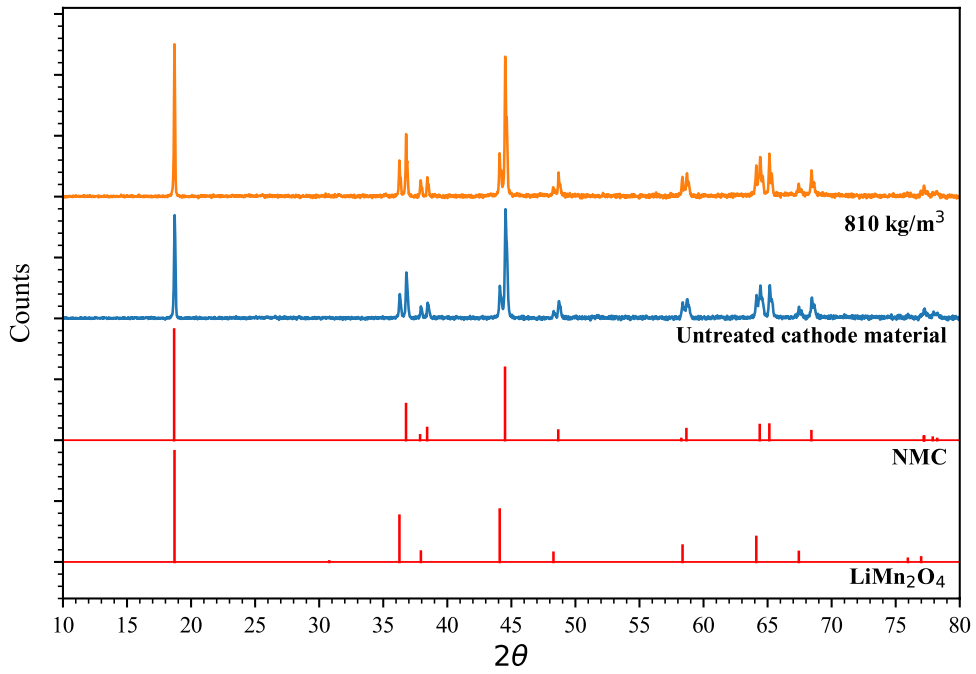

Fig. 5. : The XRD pattern of the active cathode material of an untreated sample and a sample treated at a CO_2 density of 810 kg/m^3 in the 2Θ range from 10° to 80°. The PDF card diffraction pattern from NMC, and $LiMn_2O_4$ are plotted as a reference.

[31] reported an increase in EC, and $LiPF_6$ extraction yield with the use of a co-solvent.

Finally, the impact of the proposed extraction process on the active cathode material was investigated by XRD analysis. The XRD pattern of the active cathode material of an untreated sample and a sample treated at a CO_2 density of 810 kg/m^3, where high separation yield at the highest-pressure condition (120 bar) was observed, are plotted in Fig. 5 in the 2Θ range from 10° to 80°. The PDF card diffraction lines of NMC, and $LiMn_2O_4$ are plotted as a reference. In both samples, diffraction peaks corresponding to rhombohedral structured NMC with R-3 m space group and cubic structured lithium manganese oxide ($LiMnO_4$) with Fd-3 m space group were detected. A change in the cathode active material crystal structure induced by the electrolyte solvent extraction process conditions was not observed. Hence, it is believed that the proposed pre-treatment step for the recovery of the electrolyte does not impact the cathode active material composition and crystal structure. Thus, subsequent hydrometallurgical processes to recover the valuable active materials from the LiB waste will not be negatively affected by this suggested pre-treatment step. In the contrary, the removal of the organic solvents from the LiB waste is believed to be potentially very beneficial. Literature showed that dissolved organic matter in aquatic environments impeded filtration processes, altered the interaction between metals and inorganic ligands, and can interfere precipitation of i.e., metal sulfides, and calcium carbonate [55,56].

4. Conclusion

The effect of different process conditions for sub – $scCO_2$ extraction of the electrolyte from spent EV LiB samples were investigated in this study. The CO_2 density was determined to be the significant factor for the electrolyte extraction. The highest electrolyte extraction yield of 66% was reached at a CO_2 density of 715 kg/m^3 and did not further increase with the CO_2 density. The collected extract was mainly composed of the DMC, and EMC. The polar electrolyte solvent EC, and the electrolyte degradation products DEC, DMFP, and EMFP were detected in trace amounts. Thus, the non-polar electrolyte solvents DMC, and EMC were successfully selectively extracted at the studied conditions. In the exhaust stream of the process, direct decomposition products of the conductive salt, HF, and POF_3 were not detected, but P (362 ± 65 mg/L) was detected in the extracts. The detected amount corresponds to a trace amount of $LiPF_6$ (<1.2% of 1 M $LiPF_6$) which was believed to originate from electrolyte aging products. The proposed toxic-free emission process is a promising method to selectively recover the non-polar linear carbonates DMC, and EMC from spent LIBs without the generation of secondary waste. Further research is required to investigate the extraction of the polar electrolyte components EC, and $LiPF_6$.

CRediT authorship contribution statement

Fox Robert V.: Writing – review & editing. **Zachmann Nils:** Writing – review & editing, Writing – original draft, Visualization, Validation, Software, Methodology, Investigation, Formal analysis, Data curation, Conceptualization. **Ebin Burçak:** Writing – review & editing, Supervision, Resources, Methodology, Funding acquisition, Conceptualization. **Petranikova Martina:** Writing – review & editing, Supervision.

Declaration of Competing Interest

The authors declare the following financial interests/personal relationships which may be considered as potential competing interests: Burçak Ebin reports financial support was provided by Swedish Energy Agency. Burçak Ebin reports financial support was provided by Horizon Europe. Burçak Ebin reports financial support was provided by Swedish Research Council Formas.

Data availability

The authors do not have permission to share data.

Acknowledgements

This work was supported by the Swedish Energy Agency Battery Fund Program (Project No: P2019-90078), FORMAS – Swedish Research Council for Sustainable Development (Project No: 2021–01699), and Horizon Europe (Project 101069685 — RHINOCEROS). The authors

would like to acknowledge the Chalmers Material Analysis Laboratory, CMAL, for providing their facilities and assistance for the XRD characterization.

Supportive information

Illustration of the experimental set-up, Plot representing the sample weight loss dependence on extraction time, FTIR spectra and photograph of the sample after the experiment (PDF).

Appendix A. Supporting information

Supplementary data associated with this article can be found in the online version at doi:10.1016/j.jcou.2024.102703.

References

[1] M. Li, C. Wang, Z. Chen, K. Xu, J. Lu, New concepts in electrolytes, Chem. Rev. 120 (2020) 6783–6819, https://doi.org/10.1021/acs.chemrev.9b00531.

[2] E. Mossali, N. Picone, L. Gentilini, O. Rodriguez, J.M. Pérez, M. Colledani, Lithium-ion batteries towards circular economy: a literature review of opportunities and issues of recycling treatments, J. Environ. Manag. 264 (2020) 110500, https://doi.org/10.1016/j.jenvman.2020.110500.

[3] D.L. Thompson, J.M. Hartley, S.M. Lambert, M. Shiref, G.D.J. Harper, E. Kendrick, P. Anderson, K.S. Ryder, L. Gaines, A.P. Abbott, The importance of design in lithium ion battery recycling-a critical review, Green. Chem. 22 (2020) 7585–7603, https://doi.org/10.1039/d0gc02745f.

[4] K. Xu, Nonaqueous liquid electrolytes for lithium-based rechargeable batteries, Chem. Rev. 104 (2004) 4303–4417, https://doi.org/10.1021/cr030203g.

[5] Y. Horowitz, C. Schmidt, D. Yoon, L.M. Riegger, L. Katzenmeier, G.M. Bosch, M. Noked, Y. Ein-Eli, J. Janek, W.G. Zeier, C.E. Diesendruck, D. Golodnitsky, Between liquid and all solid: a prospect on electrolyte future in lithium-ion batteries for electric vehicles, Energy Technol. 8 (2020) 2000580, https://doi.org/10.1002/ente.202000580.

[6] D. Hubble, D.E. Brown, Y. Zhao, C. Fang, J. Lau, B.D. McCloskey, G. Liu, Liquid electrolyte development for low-temperature lithium-ion batteries, Energy Environ. Sci. 15 (2022) 550–578, https://doi.org/10.1039/d1ee01789f.

[7] F. Arshad, L. Li, K. Amin, E. Fan, N. Manurkar, A. Ahmad, J. Yang, F. Wu, R. Chen, A comprehensive review of advancement in recycling anode and electrolyte from spent lithium ion batteries, ACS Sustain. Chem. Eng. 8 (2020) 13527–13554, https://doi.org/10.1021/acssuschemeng.0c04940.

[8] O. Velázquez-Martínez, J. Valio, A. Santasalo-Aarnio, M. Reuter, R. Serna-Guerrero, A critical review of lithium-ion battery recycling processes from a circular economy perspective, Batteries 5 (2019), https://doi.org/10.3390/batteries5040068.

[9] G. Harper, R. Sommerville, E. Kendrick, L. Driscoll, P. Slater, R. Stolkin, A. Walton, P. Christensen, O. Heidrich, S. Lambert, A. Abbott, K. Ryder, L. Gaines, P. Anderson, Recycling lithium-ion batteries from electric vehicles, Nature 575 (2019) 75–86, https://doi.org/10.1038/s41586-019-1682-5.

[10] X. Zhong, W. Liu, J. Han, F. Jiao, W. Qin, T. Liu, C. Zhao, Pyrolysis and physical separation for the recovery of spent LiFePO 4 batteries, Waste Manag 89 (2019) 83–93, https://doi.org/10.1016/j.wasman.2019.03.068.

[11] G. Zhang, X. Yuan, Y. He, H. Wang, W. Xie, T. Zhang, Organics removal combined with in situ thermal-reduction for enhancing the liberation and metallurgy efficiency of LiCoO2 derived from spent lithium-ion batteries, Waste Manag 115 (2020) 113–120, https://doi.org/10.1016/j.wasman.2020.05.030.

[12] S. Bertilsson, F. Larsson, M. Furlani, I. Albinsson, B.E. Mellander, Lithium-ion battery electrolyte emissions analyzed by coupled thermogravimetric/Fourier-transform infrared spectroscopy, J. Power Sources 365 (2017) 446–455, https://doi.org/10.1016/j.jpowsour.2017.08.082.

[13] F. Diaz, Y. Wang, R. Weyhe, B. Friedrich, Gas generation measurement and evaluation during mechanical processing and thermal treatment of spent Li-ion batteries, Waste Manag 84 (2019) 102–111, https://doi.org/10.1016/j.wasman.2018.11.029.

[14] X. Hu, E. Mousa, L. Ånnhagen, Z. Musavi, M. Alemrajabi, B. Hall, G. Ye, Complex gas formation during combined mechanical and thermal treatments of spent lithium-ion-battery cells, J. Hazard. Mater. 431 (2022) 128541, https://doi.org/10.1016/J.JHAZMAT.2022.128541.

[15] N.P. Lebedeva, L. Boon-Brett, Considerations on the chemical toxicity of contemporary li-ion battery electrolytes and their components, J. Electrochem. Soc. 163 (2016) A821–A830, https://doi.org/10.1149/2.0171606jes.

[16] G. Harper, P.A. Anderson, E. Kendrick, W. Mrozik, P. Christensen, S. Lambert, D. Greenwood, P.K. Das, M. Ahmeid, Z. Milojevic, W. Du, D.J.L. Brett, P. R. Shearing, A. Rastegarpanah, R. Solkin, R. Sommerville, A. Zorin, J.L. Durham, A. Abbott, D. Thompson, N. Browning, L. Mehdi, M. Bahri, F. Schnaider-Tontini, D. Nicholls, C. Stallmeister, B. Friedrich, M. Sommerfeld, L.L. Driscoll, A. Jarvis, E. C. Giles, P.R. Slater, V. Echavarri-Bravo, G. Maddalena, L. Horsfall, L. Gaines, Q. Dai, S.J. Jethwa, A.L. Lipson, G.A. Leeke, T.D. Cowell, J.G. Farthing, G. Mariani, A. Smith, Z. Iqbal, R. Golmohammadzadeh, L. Sweeney, V. Goodship, Z. Li, J. S. Edge, L. Lander, V. Nguyen-Tien, R.J.R. Elliott, O. Heidrich, M. Slattery, D. Reed, J. Ahuja, A. Cavoski, R. Lee, E. Driscoll, J. Baker, P.B. Littlewood, I. Styles, S. Mahanty, F. Boons, Roadmap for a sustainable circular economy in lithium-ion and future battery technologies, J. Phys. Energy 5 (2022) 021501, https://doi.org/10.1088/2515-7655/acaa57.

[17] Y.C. An, X.X. Gao, W.L. Jiang, J.L. Han, Y. Ye, T.M. Chen, R.Y. Ren, J.H. Zhang, B. Liang, Z.L. Li, A.J. Wang, N.Q. Ren, A critical review on graphene oxide membrane for industrial wastewater treatment, Environ. Res. 223 (2023) 115409, https://doi.org/10.1016/J.ENVRES.2023.115409.

[18] T.O. Ajiboye, O.A. Oyewo, D.C. Onwudiwe, Simultaneous removal of organics and heavy metals from industrial wastewater: a review, Chemosphere 262 (2021) 128379, https://doi.org/10.1016/J.CHEMOSPHERE.2020.128379.

[19] R. Zhang, X. Shi, O.C. Esan, L. An, Organic electrolytes recycling from spent lithium-ion batteries, Glob. Chall. (2022) 2200050, https://doi.org/10.1002/gch2.202200050.

[20] S. Nowak, M. Winter, The role of sub- and supercritical CO_2 as "processing solvent" for the recycling and sample preparation of lithium ion battery electrolytes, Molecules 22 (2017) 403, https://doi.org/10.3390/molecules22030403.

[21] P. Haas, S. Pfeifer, J. Müller, C. Bradtmöller, S. Scholl, Separation of the Electrolyte—Solvent Extraction. in: Sustain. Prod. Life Cycle Eng. Manag, Springer,, 2018, pp. 155–176, https://doi.org/10.1007/978-3-319-70572-9_9.

[22] F. Stehmann, C. Bradtmöller, S. Scholl, Separation of the Electrolyte—Thermal Drying. in: Sustain. Prod. Life Cycle Eng. Manag, Springer, 2018, pp. 139–153, https://doi.org/10.1007/978-3-319-70572-9_8.

[23] M.D.L. de Castro, M. Valcárcel, M.T. Tena, Analytical Supercritical Fluid Extraction, Springer Berlin Heidelberg, 1994, https://doi.org/10.1007/978-3-642-78673-0.

[24] K. Shanab, C. Neudorfer, H. Spreitzer, Green solvents in organic synthesis: an overview II, Curr. Org. Chem. 20 (2016) 1576–1583, https://doi.org/10.2174/1385272820666160209212804.

[25] S.P. Nalawade, F. Picchioni, L.P.B.M. Janssen, Supercritical carbon dioxide as a green solvent for processing polymer melts: processing aspects and applications, Prog. Polym. Sci. 31 (2006) 19–43, https://doi.org/10.1016/j.progpolymsci.2005.08.002.

[26] G.N. Sapkale, S.M. Patil, U.S. Surwase, P.K. Bhatbhage, SUPERCRITICAL FLUID EXTRACTION, 2010.

[27] A.I. Cooper, Polymer synthesis and processing using supercritical carbon dioxide, J. Mater. Chem. 10 (2000) 207–234, https://doi.org/10.1039/a906486i.

[28] M. Altarsha, F. Ingrosso, M.F. Ruiz-Lopez, A new glimpse into the CO_2 -philicity of carbonyl Compounds, ChemPhysChem 13 (2012) 3397–3403, https://doi.org/10.1002/cphc.201200135.

[29] P. Raveendran, Y. Ikushima, S.L. Wallen, Polar attributes of supercritical carbon dioxide, Acc. Chem. Res. 38 (2005) 478–485, https://doi.org/10.1021/ar040082m.

[30] M. Grützke, V. Kraft, W. Weber, C. Wendt, A. Friesen, S. Klamor, M. Winter, S. Nowak, Supercritical carbon dioxide extraction of lithium-ion battery electrolytes, J. Supercrit. Fluids 94 (2014) 216–222, https://doi.org/10.1016/j.supflu.2014.07.014.

[31] M. Grützke, X. Mönnighoff, F. Horsthemke, V. Kraft, M. Winter, S. Nowak, Extraction of lithium-ion battery electrolytes with liquid and supercritical carbon dioxide and additional solvents, RSC Adv. 5 (2015) 43209–43217, https://doi.org/10.1039/c5ra04451k.

[32] W.E. Org, Y. Liu, D. Mu, Y. Dai, Q. Ma, R. Zheng, C. Dai, Analysis on extraction behaviour of lithium-ion battery electrolyte solvents in supercritical CO 2 by gas chromatography, Int. J. Electrochem. Sci. 11 (2016) 7594–7604, https://doi.org/10.20964/2016.09.03.

[33] D. Mu, Y. Liu, R. Li, Q. Ma, C. Dai, Transcritical CO_2 extraction of electrolytes for lithium-ion batteries: optimization of the recycling process and quality-quantity variation, N. J. Chem. 41 (2017) 7177–7185, https://doi.org/10.1039/c7nj00771j.

[34] N. Zachmann, M. Petranikova, B. Ebin, Electrolyte recovery from spent Lithium-Ion batteries using a low temperature thermal treatment process, J. Ind. Eng. Chem. 118 (2022) 351–361, https://doi.org/10.1016/j.jiec.2022.11.020.

[35] K.D. Bartle, T. Boddington, A.A. Clifford, S.B. Hawthorne, The effect of solubility on the kinetics of dynamic supercritical-fluid extraction, J. Supercrit. Fluids 5 (1992) 207–212, https://doi.org/10.1016/0896-8446(92)90009-9.

[36] S.B. Hawthorne, A.B. Galy, V.O. Schmitt, D.J. Miller, Effect of SFE flow rate on extraction rates: classifying sample extraction behavior, Anal. Chem. 67 (1995) 2723–2732, https://doi.org/10.1021/ac00111a034.

[37] H.J. Vandenburg, A.A. Clifford, K.D. Bartle, J. Carroll, I. Newton, L.M. Garden, J. R. Dean, C.T. Costley, Analytical extraction of additives from polymers, Analyst 122 (1997) 101R–116R, https://doi.org/10.1039/a704052k.

[38] Online - Calculation - Carbon dioxide, (n.d.). https://www.peacesoftware.de/einigewerte/co2_e.html (accessed January 24, 2023).

[39] X. Mönnighoff, A. Friesen, B. Konersmann, F. Horsthemke, M. Grützke, M. Winter, S. Nowak, Supercritical carbon dioxide extraction of electrolyte from spent lithium ion batteries and its characterization by gas chromatography with chemical ionization, J. Power Sources 352 (2017) 56–63, https://doi.org/10.1016/j.jpowsour.2017.03.114.

[40] J. Henschel, F. Horsthemke, Y.P. Stenzel, M. Evertz, S. Girod, C. Lürenbaum, K. Kösters, S. Wiemers-Meyer, M. Winter, S. Nowak, Lithium ion battery electrolyte degradation of field-tested electric vehicle battery cells – A comprehensive analytical study, J. Power Sources 447 (2020) 227370, https://doi.org/10.1016/j.jpowsour.2019.227370.

[41] V. Kraft, M. Grützke, W. Weber, M. Winter, S. Nowak, Ion chromatography electrospray ionization mass spectrometry method development and investigation of lithium hexafluorophosphate-based organic electrolytes and their thermal decomposition products, J. Chromatogr. A. 1354 (2014) 92–100, https://doi.org/10.1016/j.chroma.2014.05.066.

[42] H. Yang, G.V. Zhuang, P.N. Ross, Thermal stability of LiPF6 salt and Li-ion battery electrolytes containing LiPF6, J. Power Sources 161 (2006) 573–579, https://doi.org/10.1016/j.jpowsour.2006.03.058.
[43] Y. Yuan, A.S. Teja, Quantification of specific interactions between CO_2 and the carbonyl group in polymers via ATR-FTIR measurements, J. Supercrit. Fluids 56 (2011) 208–212, https://doi.org/10.1016/j.supflu.2010.12.010.
[44] F. Ingrosso, M.F. Ruiz-López, Modeling solvation in supercritical CO_2, ChemPhysChem 18 (2017) 2560–2572, https://doi.org/10.1002/cphc.201700434.
[45] D. Kajiya, M. Imanishi, K.I. Saitow, Solvation of Esters and ketones in supercritical CO_2, J. Phys. Chem. B. 120 (2016) 785–792, https://doi.org/10.1021/acs.jpcb.5b11740.
[46] M. Anouti, Y. Rodrigue Dougassa, C. Tessier, L. El Ouatani, J. Jacquemin, Low pressure carbon dioxide solubility in pure electrolyte solvents for lithium-ion batteries as a function of temperature, Meas. Predict. (2012), https://doi.org/10.1016/j.jct.2012.01.027.
[47] Z. Piao, R. Gao, Y. Liu, G. Zhou, H.M. Cheng, A review on regulating Li+ solvation structures in carbonate electrolytes for lithium metal batteries, Adv. Mater. 35 (2023) 2206009, https://doi.org/10.1002/ADMA.202206009.
[48] S.J. Jethwa, L.A. Román-Ramírez, P.A. Anderson, G.A. Leeke, Vapor equilibrium data for the binary mixtures of dimethyl carbonate and ethyl methyl carbonate in compressed carbon dioxide, Int. J. Thermophys. 44 (2023) 1–13, https://doi.org/10.1007/S10765-023-03186-2/FIGURES/4.
[49] M.H. Lee, J.H. Yim, J.W. Kang, J.S. Lim, Measurement of VLE data of carbon dioxide + dimethyl carbonate system for the direct synthesis of dimethyl carbonate using supercritical CO_2 and methanol, Fluid Phase Equilib. 318 (2012) 77–82, https://doi.org/10.1016/J.FLUID.2012.01.020.
[50] R. Piñero, J. García, M. Sokolova, M.J. Cocero, Modelling of the phase behaviour for the direct synthesis of dimethyl carbonate from CO_2 and methanol at supercritical or near critical conditions, J. Chem. Thermodyn. 39 (2007) 536–549, https://doi.org/10.1016/J.JCT.2006.09.009.
[51] S. Camy, J.S. Pic, E. Badens, J.S. Condoret, Fluid phase equilibria of the reacting mixture in the dimethyl carbonate synthesis from supercritical CO_2, J. Supercrit. Fluids 25 (2003) 19–32, https://doi.org/10.1016/S0896-8446(02)00087-6.
[52] F. Bustamante, A.F. Orrego, S. Villegas, A.L. Villa, Modeling of chemical equilibrium and gas phase behavior for the direct synthesis of dimethyl carbonate from CO 2 and methanol, Ind. Eng. Chem. Res. 51 (2012) 8945–8956, https://doi.org/10.1021/IE300017R/SUPPL_FILE/IE300017R_SI_001.PDF.
[53] R.P. Ciccolini, A.C. Madlinger, S.A. Rogers, J.W. Tester, Vapor - Liquid equilibrium data and predictive correlations for the carbon dioxide - Dimethyl carbonate binary mixture, J. Chem. Eng. Data. 55 (2010) 2673–2681, https://doi.org/10.1021/JE900948N/SUPPL_FILE/JE900948N_SI_001.PDF.
[54] C.H. Cheng, Y.P. Chen, Vapor–liquid equilibria of carbon dioxide with isopropyl acetate, diethyl carbonate and ethyl butyrate at elevated pressures, Fluid Phase Equilib. 234 (2005) 77–83, https://doi.org/10.1016/J.FLUID.2005.05.018.
[55] J. Yang, T. Retegan, C. Ekberg, Indium recovery from discarded LCD panel glass by solvent extraction, (2013). https://doi.org/10.1016/j.hydromet.2013.05.008.
[56] G.R. Aiken, H. Hsu-Kim, J.N. Ryan, Influence of dissolved organic matter on the environmental fate of metals, nanoparticles, and colloids, Environ. Sci. Technol. 45 (2011) 3196–3201, https://doi.org/10.1021/ES103992S/ASSET/IMAGES/LARGE/ES-2010-03992S_0001.JPEG.